Experimental evidence of a strong image force between highly charged electrosprayed molecular ions and a metal screen

doi: 10.4209/aaqr.2016.04.0147

Experimental evidence of a strong image force between highly charged electrosprayed molecular ions and a metal screen

Youichi Omori[1], Hyun-Jin Choi[2] Yasuaki Mukai[2], Toshiyuki Fujimoto[3], Tomoya Tamadate[2], Takafumi Seto[2], Yoshio Otani[2], and Mikio Kumita[2*]

[1] Sanzen Seishi Co. Ltd., Kanaiwa-kita, Kanazawa, Ishikawa 920-0338, Japan
[2] School of Natural System, College of Science and Engineering, Kanazawa University, Kakuma-machi, Kanazawa, Ishikawa 920-1192, Japan
[3] Department of Applied Sciences, Muroran Institute of Technology, 27-1 Mizumoto-cho, Muroran, Hokkaido 050-8585, Japan

Abstract

We investigated the capturing mechanisms of highly charged macromolecular ions of polyethylene glycol electrosprayed onto a metal screen. Our experiments assessed how the charge state, size of the macromolecular ions, and filtration velocity affected the penetration of the ions through the metal screen. The single fiber efficiencies were plotted as functions of the Peclet number and image force parameter. Highly charged molecular ions had much higher collection efficiencies than neutralized macromolecules, suggesting the presence of a strong image force between the ions and metal surface. The single fiber efficiency by image force was proportional to the square root of an image force parameter predicted by theory. When using the prefactor of 9.7 proposed by Alonso *et al*. (2007), we found fair agreement between the experimental data and theoretical predictions on the collection efficiency of highly charged molecular ions with mobility diameters from 2.6 to 4.8 nm and numbers of electrical charges from 2 to 7. The experimental evidence from our study reveals that image force contributes strongly to the collection of multicharged macromolecular ions by a metal wire screen.

Keywords: Image force, Metal screen, Electrospray, Molecular ion

*Corresponding author. Tel: 81-76-234-4827; Fax: 81-76-234-4826
E-mail address: kumita@se.kanazawa-u.ac.jp

INTRODUCTION

When a charged particle approaches a neutral solid surface, a short-range force between the particle and induced dipole, a so-called “image force”, is created. Image force is a well-known mechanism of particle collection by air filters (Brown, 1993), especially when the particles possess a high number of charges (Yoshioka *et al*., 1968) or the particle size falls in the nanometer range (Alonso *et al*., 2007; Heim *et al*., 2010). Yoshioka *et al*. (1968) measured the collection efficiency of electrically charged oil droplets with a 1 μm diameter by a neutral glass fiber filter. The number of charges per droplet was controlled using a pin-to-plate type discharge electrode. The collection efficiency of 60-charged particles (1 μm) was about 40 % higher than that of uncharged particles in their experiment. Lundgen and Whitby (1965) measured the collection efficiency of highly charged (−300 to +320 elemental charges) particles with 0.1 and 1 μm diameters using electrically neutral filters made of felt, urethane, and glass fiber. They reported that the collection efficiency increased from 16 % (uncharged particles) to over 99 % when the particles carried +320 electrical charges. To evaluate the effect of image force in a diffusion limited regime (image force parameter, $K_{IM} < 10^{-5}$), Alonso *et al*. (2007) experimentally measured the collection efficiency of nanoparticles ($ZnCl_2$ and NaCl) with diameters from 25 to 65 nm by a metal screen (aluminum and stainless steel). The image force had contributed significantly to the mechanism by which the charged nanoparticles, even the particles with small numbers of electrical charges, were collected in their experiment.

As reported in previous studies, image force has a significant influence on the mechanism by which highly charged nanoparticles are collected. Few reports, however, have investigated the effect of image force on the collection of very small particles (< 10 nm). New factor to consider emerge in a size regime of < 10 nm, such as the thermal rebound (Wang and Kasper, 1991) and

the effects of Brownian diffusion and image force in combination (Alonso *et al*., 2007). Heim *et al*. (2010) investigated the collection efficiencies of tungsten oxides nanoparticles (1.2 to 8 nm, neutral and monovalent) and electrosprayed molecular ions by metal meshes (nickel and stainless steel). The efficiencies of nanoparticle collection in their experiments were in good agreement with the predicted collection efficiency of particles with diameters larger than 3 nm. They also found, however, that image force has only a minor effect on the collection efficiency of nanoparticles, because the number of charges of their test particles was unity.

We studied the effect of image force on the particle collection in the course of investigation of thermal rebound of sub-10 nm particles. Since we have neither definite generation method nor the measurement methods for sub-10 nm particles, we employed macromolecular ions as a monodisperse test particles generated by an electrospray, which is a powerful tool for producing molecular ions (Yamashita *et al*., 1984). However, we found that the electrospray generates highly charged macromolecular ions so that the collection efficiency of these ions was significantly affected by the image force. Consequently, we must account for the image force in the interpretation of collection efficiency data for elucidating the thermal rebound of sub-10 nm particles.

In the present study, we generated highly charged polyethylene glycol (PEG) molecular ions (from +2 to +7) with diameters below 5 nm by an electrospraying PEG with various molecular weights. We measured the collection efficiency of highly charged molecular ions through wire screens as a function of mobility diameters and numbers of charges and compared the experimental data with the empirical equation reported by Alonso *et al*. (2007) in order to examine whether the empirical equation obtained for particles larger than 10 nm holds for sub-10 nm particles.

COLLECTION OF CHARGED NANOPARTICLES BY IMAGE FORCE

The influences of image force were evaluated by a dimensionless image force parameter, K_{IM}, given by

$$K_{IM} = \left(\frac{\varepsilon_f - 1}{\varepsilon_f + 2}\right)\frac{Cq^2e^2}{12\pi^2\mu u\varepsilon_0 d_p d_f^2} \quad (1)$$

where, ε_f and ε_0 are dielectric constants of the fiber and vacuum, C is the Cunningham slip correction factor, q is the number of charges on the particle, e is the elementary charge, μ is the air viscosity, u is the air flow velocity, d_p is the particle diameter, d_f is the fiber diameter. Single fiber efficiency by image force is known to be proportional to the square root of K_{IM} such that,

$$\eta_{IM} = \alpha\sqrt{K_{IM}} \quad (2)$$

where, α is a constant of proportionality, which takes different value in different reports. When Yoshioka *et al*. (1968) measured the collection efficiency of dioctyl phthalate by a glass filter mat, they reported an α value of 2.3 from experiments using 1 mm particles ($10^{-6} < K_{IM} < 10^{-3}$). A few years earlier, Lundgen and Whitby (1965) reported an α value of 1.5 from experiments on solid spherical aerosol particles with diameter ranging from 0.1 μm to 1 μm ($2\times10^{-6} < K_{IM} < 3\times10^{-2}$). In the diffusion regime, the total single fiber efficiency, η_T, is expressed as the sum of the single fiber efficiencies of diffusion, image force, and the combined effect of diffusion and image force as,

$$\eta_T = \eta_D + \eta_{IM} + \eta_{DIM} \quad (3)$$

The single fiber collection efficiency of diffusion, η_D is expressed by the following equation (Cheng and Yeh, 1980):

$$\eta_D = 2.7 Pe^{-2/3} \quad (4)$$

where, Pe is the Peclet number given by

$$Pe = \frac{u d_f}{D} \quad (5)$$

where D is the diffusion coefficient. The third term of Eq. (3), η_{DIM}, is the single fiber efficiency by a combination of two capturing mechanisms, diffusion and image force.

Alonso *et al*. (2007) found that the pure image force effect was negligible in the diffusion regime ($200 < Pe < 3600$, $10^{-7} < K_{IM} < 10^{-5}$) and obtained the following equation for η_{DIM} (combined effect):

$$\eta_{DIM} = 29.7 K_{IM}^{0.59} \quad (6)$$

They also fitted the experimental data by assuming that η_{DIM} was proportional to the square root of the K_{IM}, and it also shows reasonable agreement between the experimental data when α = 9.7 as follows:

$$\eta_{DIM} = 9.7\sqrt{K_{IM}} \quad (7)$$

Fig. 1 shows the size dependency of single fiber efficiency by image force, η_{IM}, calculated by Eq. (7) with changing numbers of charges, q (u = 0.25 m s^{-1}). The solid line and dashed lines respectively represent the single fiber efficiency by pure diffusion and by diffusion and image force combined. As the figure shows, the single fiber efficiency increases with q and decreases with the particle diameter. The image force effect is clearly significant when the particles carry more than several electrical charges. Highly charged nanoparticles of this type can be generated by electrospray atomization.

METHODS

Preparation of multicharged PEG molecular ions

Fig. 2 shows the experimental setup used in this study. Highly charged electrosprayed molecular ions were used as test particles in the filtration experiments. Polyethylene glycol (PEG) with the monodispersed molecular weight from 2,000 to 21,300 were purchased from Sigma Aldrich (M_W = 10000), Wako (M_W = 2000, 4600) and Agilent Technologies (M_W = 21300). PEG (0.005 to 0.043 wt%) and 0.1 wt% ammonium acetate were dissolved in a water/methanol (50:50) solution for the electrospray atomization. The mixture of water/methanol solution, and the addition of ammonium acetate have been widely employed in order to increase the electrical conductivity of precursor solution in electrospray process (Lenggoro *et al*., 2002). In addition, the correlations between PEG concentration and charging state were reported in our previous research (Maekawa *et al*., 2014).

148 The PEG solution was introduced to the capillary (Hamilton, Model 7747-02, inner diameter of
149 110 μm, outer diameter of 240 μm) via a syringe pump at a constant flow rate of 100 to 200 μL
150 h^{-1}. High voltage (2.5 to 3 kV) was applied to the capillary to obtain a stable cone jet under
151 observation by a CCD camera (Sony, Model XC-75). as shown in Fig. 3. The gap distance
152 between syringe tip to electrical ground was set to 0.3 cm. The generated droplets were carried by
153 dry clean air at flow rate of 3 to 5 L min^{-1}. Part of the gas flow was introduced into a differential
154 mobility analyzer (DMA) (Laboratory-made, Vienna type, Winklmayr *et al*. 1991) to obtain
155 mono-mobility particles. The number concentrations of the DMA classified particles were
156 monitored using a condensation particle counter (CPC) (TSI, Model 3776, Fig. 2(a)).
157 The charging state of the test particles was investigated by introducing the DMA-classified
158 PEG molecular ions to a neutralizer (^{241}Am) and measuring the mobility distribution of the
159 neutralized PEG molecules measured by a Nano-SMPS (TSI, Model 3085 nano-DMA and the
160 CPC, Fig. 2(b)). At the test particles were very small (< 5 nm), the molecular ions classified by
161 the Nano-SMPS were assumed to be monovalent. The number of electrical charges of the PEG
162 ions could therefore be estimated as a function of the diameter by changing the 1st DMA voltage
163 (for mobility scanning) and measuring the size distributions of the ions with the Nano-SMPS.
164
165 ***Evaluation of collection efficiency***
166 Mobility-classified molecular ions of known sizes and numbers of charges were introduced to
167 the filtration experiment system. Fig. 4 shows the experimental setup for measuring the filtration
168 efficiency. The effect of the image force in the diffusion regime was assessed by comparing the
169 penetration data of highly charged PEG ions (Fig. 4(a)) with the penetration data of neutralized
170 PEG molecules (Fig. 4(b)). The diffusional loss of the ions during transport was cancelled by
171 measuring the penetration using two identical filter holders (Alonso *et al*., 2007; Heim *et al*.,

2010) arranged shown in Fig. 4. Most of the tubes and connections were made of metal (electrically grounded) and set at the shortest possible lengths to minimize the diffusional loss of ions during transport.

A stainless steel (SUS) screen (fiber diameter, d_f = 30 μm, packing density, α = 0.177) was installed in one of the filter holders for use as the model filter. The diameter of the effective filtration area was 24 mm. The filtration velocity was adjusted from 0.25 to 0.40 m s^{-1} by adding clean makeup air before the ions entered the filter holders. The flow was switched between the filter and the blank holder by three-way valves. The number concentration with and without filtration was measured by the CPC.

RESULTS AND DISCUSSION

Characterization of the charged molecular ions

Fig. 5 shows contour plots of the electrical mobility (multicharged particles measured by the 1st DMA) against the particle diameter (singly charged particles measured by the 2nd DMA) for (a) PEG2000, (b) PEG4600, (c) PEG10000, and (d) PEG21300. The number concentration is represented as a difference of color (red is the highest concentration). Each of upper panels shows the CPC count plotted against particle diameters measured by directly introducing electrosprayed ions into the Nano-SMPS with a neutralizer. Two kinds of products were identified in the size distributions. The first peak observed at the smaller particle sizes could be attributed to single molecular ions, since the diameter of these first peaks increased with the increasing molecular weight of the PEG. The second peak was thought to be composed of residual nanoparticles generated by the drying of the electrosprayed droplets containing multiple PEG molecules. The diameter of this peak increased with increasing concentrations of the PEG solutions.

196 Only the molecular ions from the first peaks were used as test particles for the filtration
197 experiment, as the particles in the second peak may have been mixtures of multicharged residual
198 particles of various sizes and numbers of charges. Each of the solid lines in Fig. 5 represents the
199 relationship between the electrical mobility of the particles, Z_p, and the particle diameter, d_p, as a
200 function of the number of charges, q, given by the following Eqs. (8) and (9):
201
202 $$Z_p = \frac{qeC(d_p)}{3\pi\mu d_p} \tag{8}$$
203
204 $$C = 1 + \frac{2\lambda}{d_p}\left[1.246 + 0.420\exp\left(-0.87\frac{d_p}{2\lambda}\right)\right] \tag{9}$$
205
206 where C is the slip correction factor, and λ is the mean free path.
207 By comparing the lines with contour plots we find, that the PEG ions have 2 to 7 charges,
208 depending on the molecular weight. Table 1 summarizes the relationship of the molecular weight
209 with the mobility diameter and number of electrical charges. Disappointingly, the resolution of
210 the 1st DMA used for mobility classification was too low to accurately classify molecular ions
211 with the different numbers of charges (Saucy *et al*. 2004). Its resolution was sufficient, however,
212 to eliminate residual nanoparticles, as shown in Fig. 5. We therefore compared our experimental
213 data with the theoretical values by assuming that all of the test particles had the same number of
214 charges (see Table 1).
215
216 ***Collection of highly charged molecular ions***
217 Fig. 6 shows penetration data of the four PEG species through an SUS wire screen with and
218 without electrical neutralization at filtration velocities of 0.25 m s^{-1}. The solid line and dashed

line represent the theoretical penetration curves for uncharged and singly charged macromolecules, respectively. As the figure shows, experimentally obtained penetration of neutralized macromolecules (solid circles) decreases with decreasing diameter, which suggests that the main capturing mechanism is diffusion. It also shows fair agreement with the predicted penetration data for uncharged macromolecules (only diffusion) or singly charged ions. When the charged particles are neutralized to the equilibrium charging state, the fractions of the charged particles are estimated to be about 1% for 2 nm and 3% for 5 nm particles by Fuchs' charging theory (Fuchs, 1963). From these estimates, conclude that the experimentally obtained penetration values should closely agree with the predicted curve for uncharged macromolecules. We find, however, that the predicted curve diverges from the experimentally obtained values, possibly due to the residual electrical charge on the particles. On the other hand, we clearly see that the multicharged ions (open circles) have a much lower penetration than the neutralized species. We attribute this result to the significant contribution of the image force between the multicharged particles and SUS wire screen.

To analyze the effect of image force, we converted the penetration, P, to the single fiber efficiency, η, given by Eq. (10):

$$P = \exp\left(-\frac{4}{\pi}\frac{\alpha}{1-\alpha}\frac{L}{d_{\mathrm{f}}} n_{\mathrm{screen}} \eta \right) \tag{10}$$

where α is the packing density of the wire screen, L is thickness of wire screen, and n_{screen} is number of wire screen. Fig. 7 shows the experimental single fiber efficiencies of neutralized macromolecules and multiply charged ions obtained from Eq. (10), plotted as functions of the Peclet number, Pe (Eq. (5)). Each symbol in Fig. 7 represents the series of data for the specific

molecular weights of PEG (shown in Table 1) with changing filtration velocity. The experimental single fiber efficiency of the multicharged species (open symbols) showed various tendencies at different molecular weights (diameters) and charge states. In contrast, the single fiber efficiencies of the neutralized macromolecules determined experimentally (closed symbols) could almost be summarized into a straight line as a function of *Pe* and agreed fairly well with the predicted efficiencies for both neutralized (solid line) and singly charged ions (broken line), as previously mentioned. The broken, dashed, and dotted lines in Fig. 7 represent the theoretical single fiber efficiencies for multicharged ions (1 to 11 charges) obtained from the sum of Eqs. (4) and (7). As previously mentioned (Fig. 5), the numbers of charges obtained experimentally were 4.4 for PEG_{4600}, 6.4 for PEG_{1000}, and 7.2 for PEG_{21300}. As the figure illustrates, the experimental single fiber efficiencies of multicharged ions increased with increasing number of charges and agreed fairly well with the predicted lines with corresponding numbers of charges. This result provides quantitative evidence of a strong image force between the multicharged molecular ions and the SUS wire screen even in the diffusion regime.

To reiterate, Alonso *et al*. (2007) reported that a prefactor α of 9.7 validly applied to estimation of the image force for multicharged (maximum 3) nanoparticles in the diffusion regime (mobility diameters from 25 to 60 nm). In the present study, we extend the validation of the prefactor down to molecular ions as small as 2.6 nm (Fig. 6). In contrast, Heim *et al*. (2010) performed filtration experiments for singly charged nanoparticles in the diameter range from 1.2 to 8 nm using a metal screen. The dominance of Brownian diffusion as the mechanism of particle capture in their experiment reduced the contribution of pure image force to a negligible level. They tentatively explained this dominant effect of Brownian diffusion by the weak image force it for small numbers of charges (single), a phenomenon identified in Fig. 7 (the small difference between neutral and singly charged particles).

In summary, Fig. 8 plots the single fiber efficiency for the charged particles (the sum of pure image force plus image force and diffusion in combination), η_{IM} (= $\eta_T - \eta_D$), as a function of the image force parameter K_{IM}. Our experimental data and Alonso's results are plotted as open symbols, and closed symbols, respectively. The solid line represents the single fiber efficiency predicted by Eq. (7). As the figure shows, our experimental results agree fairly well with the line predicted by Alonso's prefactor of 9.7. Our study confirms that Alonso's prefactor of 9.7 can be applied in our experimental ranges (d_p = 2.6 ~ 4.8 nm, q = 2 ~ 7), which correspond to $10^{-3} < K_{IM} < 10^{-2}$.

CONCLUSIONS

We prepared multicharged ions carrying 2 to 7 elementary charges by an electrospray method, and investigate the mechanism by which they were collected by a SUS wire screen. The multicharged molecular ions had lower penetration than the neutralized molecules due to the image force acting between the multicharged molecular ions and SUS wire screen. The single fiber efficiency by image force also turned out to be proportional to the square root of an image force parameter predicted by theory, and the experimental and theoretical values showed fair agreement when we using the prefactor of 9.7 proposed by Alonso et al., even in the K_{IM} ranges from 10^{-3} to 10^{-2}. This study demonstrates the strong contribution of image force in the collection of multicharged molecular ions by an SUS wire screen.

REFERENCES

289 Alonso, M., Alguacil, F.J., Santos, J.P., Jidenko, N. and Borra, J.P. (2007). Deposition of ultrafine
290 aerosol particles on wire screens by simultaneous diffusion and image force. *J. Aerosol Sci.* 38:
291 1230-1239.
292 Brown, R.C. (1993). *Air filtration: An integrated approach to the theory and applications if*
293 *fibrous filters,* Pergamon Press, Oxford.
294 Cheng, Y.S. and Yeh, H.C. (1980). Theory of a screen-type diffusion battery. *J. Aerosol Sci.* 11:
295 313-320.
296 Fuchs, N.A. (1963). On the stationary charge distribution on aerosol particles in a bipolar ionic
297 atmosphere. *Geofis. Pura. Appl*. 56: 185-193.
298 Heim, M., Attoui, M. and Kasper, G. (2010). The efficiency of diffusional particle collection onto
299 wire grids in the mobility equivalent size range of 1.2-8 nm. *J. Aerosol Sci.* 41: 207-222.
300 Lundgren, D.B. and Whitby, K.T. (1965). Effect of particle electrostatic charge on filtration by
301 fibrous filters. *Ind. Eng. Chem. Process Des. Dev.* 4: 345-349.
302 Lenggoro, I. W., Xia, B., Okuyama, K., and De la Mora, J. F. (2002). Sizing of colloidal
303 nanoparticles by electrospray and differential mobility analyzer methods. *Langmuir*, 18: 4584-
304 4591.
305 Maekawa, T., Tokumi, T., Higashi, H., Seto, T. and Otani, Y. (2014). Effect of solution
306 concentration on breakup of electro-sprayed droplets and emission of solute ions. *Kagaku*
307 *Kogaku*, 40: 5-11.
308 Saucy, D.A., Ude, S., Lenggoro, I.W. and De la Mora, J.F. (2004). Mass analysis of water-soluble
309 polymers by mobility measurement of charge-reduced ions generated by electrosprays. *Anal.*
310 *Chem.* 76: 1045-1053.
311 Wang, H.C. and Kasper, G. (1991). Filtration efficiency of nanometer-size aerosol particles. *J.*
312 *Aerosol Sci.* 1: 31-41.

313 Winklmayr, W., Reischl, G.P., Lindner, A.O. and Berner, A. (1991). A new electromobility
314 spectrometer for the measurement of aerosol size distributions in the size range from 1 to 1000
315 nm. *J. Aerosol Sci*. 22: 289-296.
316 Yamashita, M. and Fenn, J.B. (1984). Electrospray ion source. Another variation on the free-jet
317 theme. *J. Phys. Chem*. 88: 4451-4459.
318 Yoshioka, N., Emi, H., Hattori, M. and Tamori, I. (1968). Effect of electrostatic force in the
319 filtration efficiency of aerosols. *Kagaku Kogaku* 32: 815-820.
320

Table Titles

Table 1. Mobility diameters and charging characteristics of PEG ions.

323 **Table 1.** Mobility diameters and charging characteristics of PEG ions.

Molecular weight of PEG [g/mol]	Concentration of PEG [wt%]	Mobility diameter [nm]	Number of charges [-]	Average number of charges [-]
2,000	0.005	2.6	1~2	2.25
4,600	0.023	3.1	2~7	4.38
10,000	0.02	4.1	3~9	6.37
21,300	0.043	4.8	5~12	7.27

324

Figure Captions

Fig. 1. Single fiber collection efficiency by diffusion and by image force.

Fig. 2. Experimental setup to prepare the PEG ions.

Fig. 3. Microscopic image of the cone-jet.

Fig. 4. Experimental setup to measure the collection efficiency.

Fig. 5. CPC count and tandem result of PEG ions.

Fig. 6. Penetration of PEG ions as a function of mobility diameter.

Fig. 7. Single fiber collection efficiencies of PEG ions as functions of the Peclet number.

Fig. 8. Single fiber efficiency by image force with Alonso's prefactor.

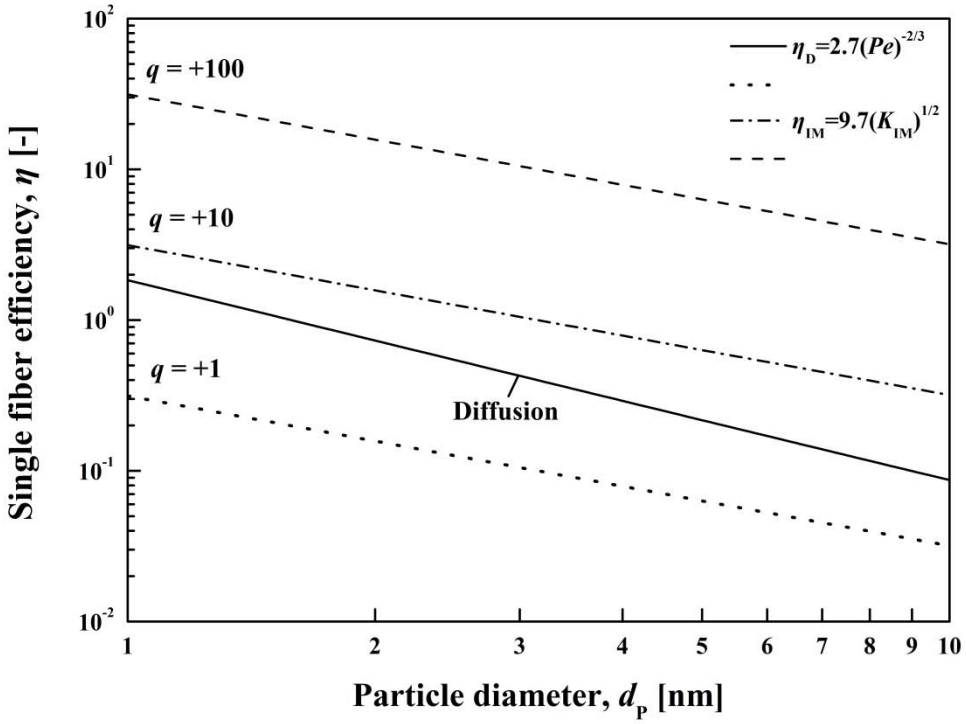

335

336 **Fig. 1.**

337

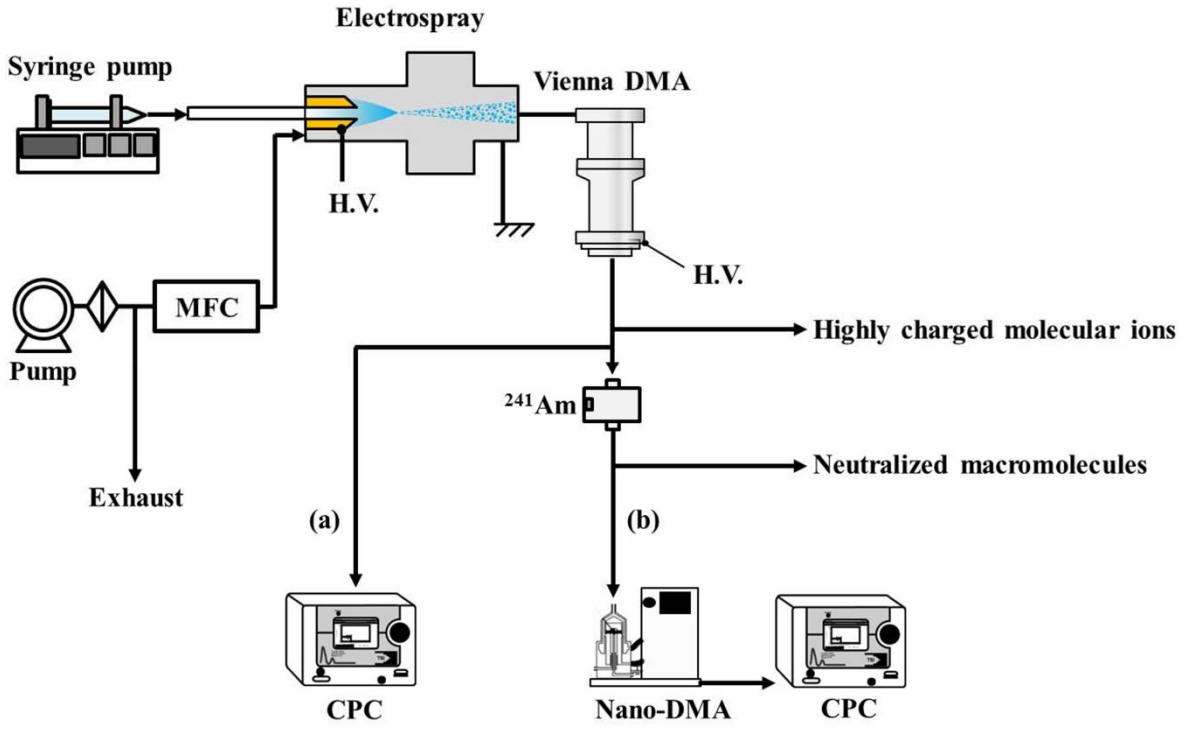
Electrospray
Syringe pump
Vienna DMA
H.V.
H.V.
MFC
Pump
Highly charged molecular ions
241Am
Neutralized macromolecules
Exhaust
(a)
(b)
CPC
Nano-DMA
CPC

338

339 **Fig. 2.**

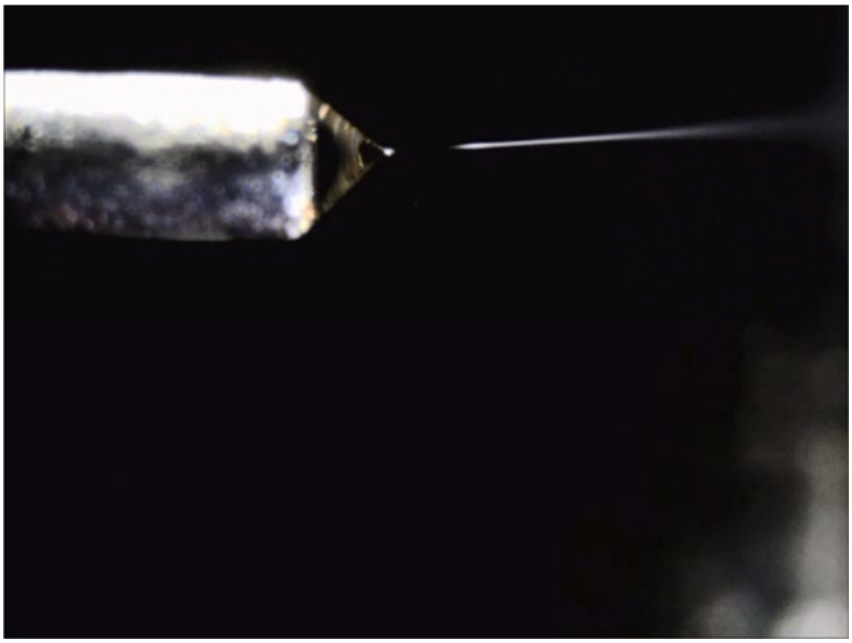

Fig. 3

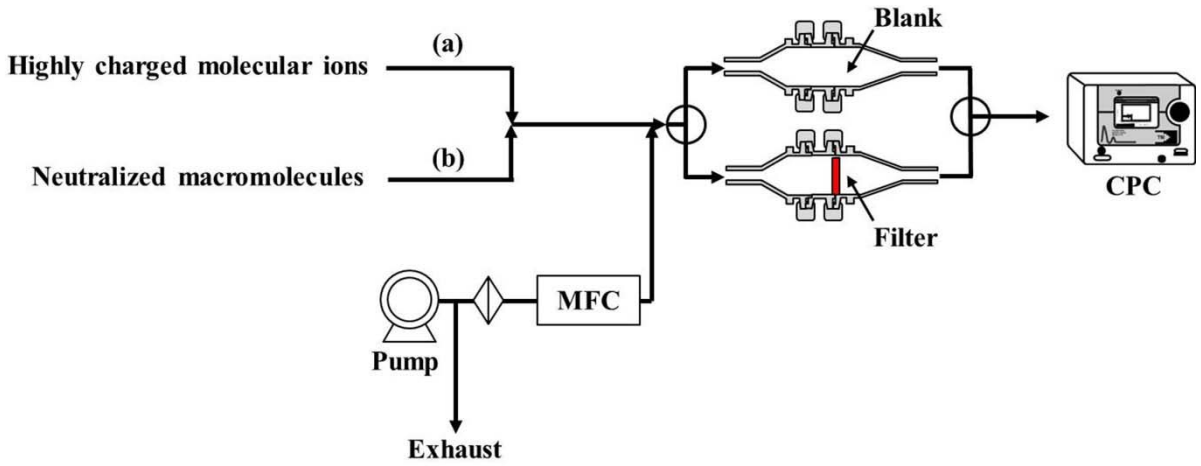
Highly charged molecular ions
(a)
Neutralized macromolecules
(b)
Blank
Filter
CPC
MFC
Pump
Exhaust

342

343 **Fig. 4.**

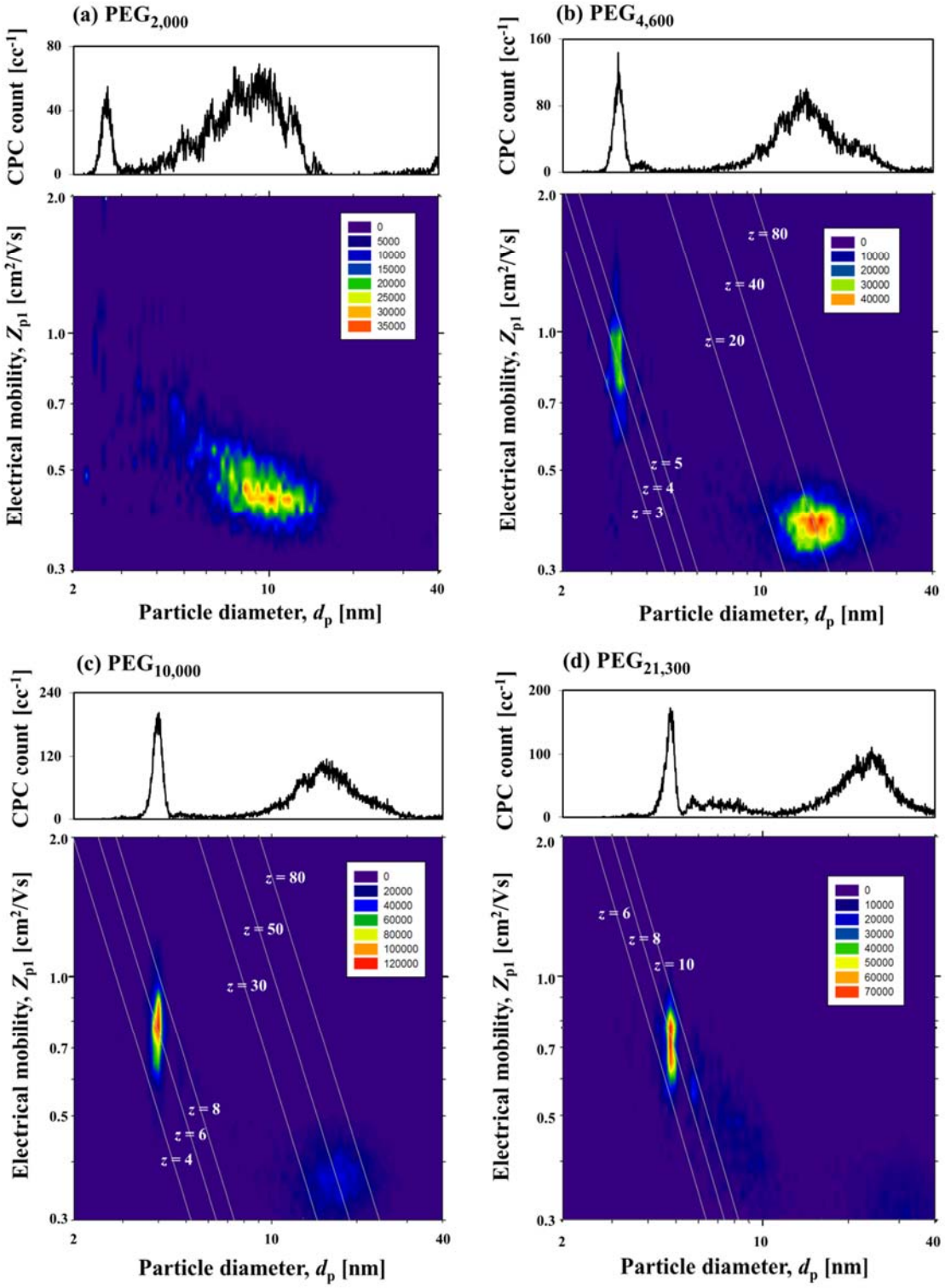
(a) PEG2,000
(b) PEG4,600
(c) PEG10,000
(d) PEG21,300
CPC count [cc-1]
Electrical mobility, Zp1 [cm2/Vs]
Particle diameter, dp [nm]
z = 80
z = 40
z = 20
z = 5
z = 4
z = 3
z = 50
z = 30
z = 8
z = 6
z = 10

344

345 **Fig. 5.**

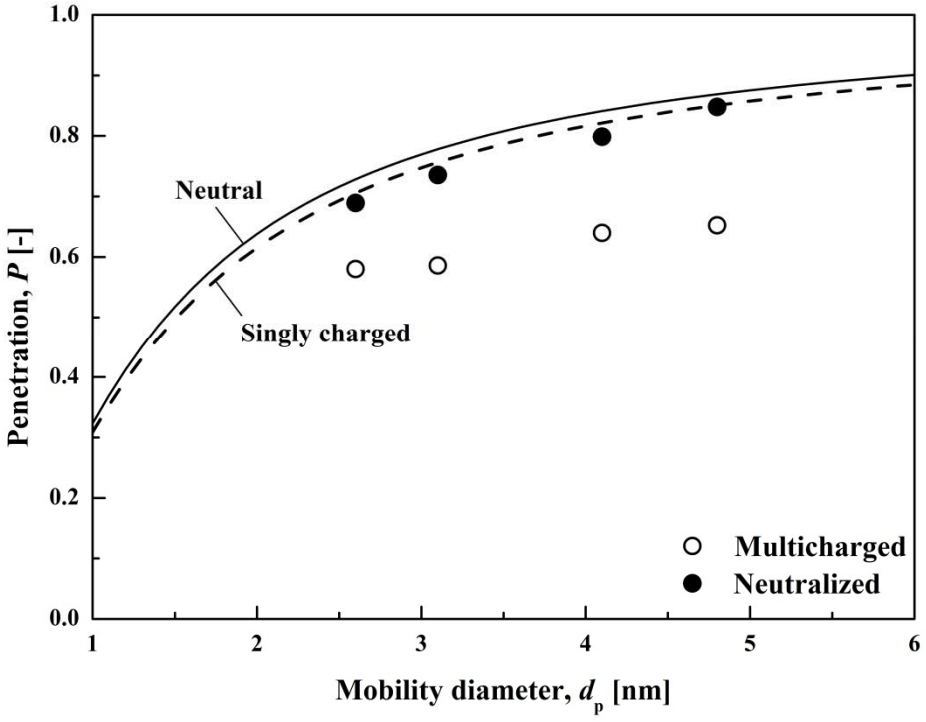
1.0
0.8
0.6
0.4
0.2
0.0
Penetration, P [-]
Neutral
Singly charged
Multicharged
Neutralized
1
2
3
4
5
6
Mobility diameter, d_p [nm]

346

347 **Fig. 6.**

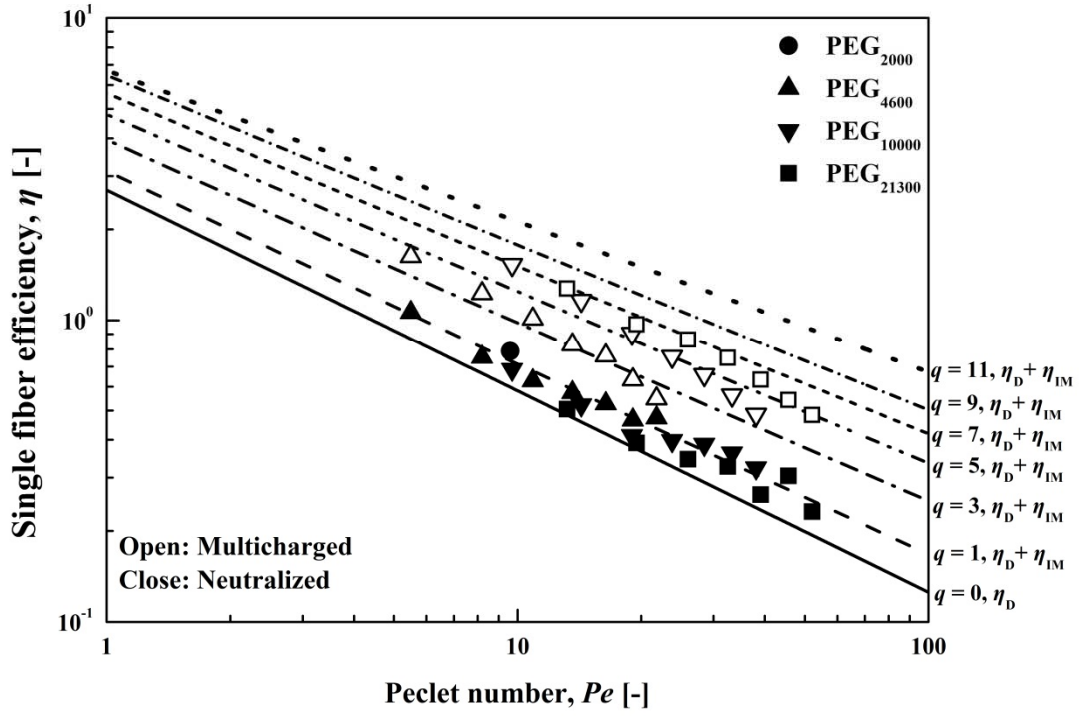
Single fiber efficiency, η [-]
Peclet number, Pe [-]
PEG2000
PEG4600
PEG10000
PEG21300
Open: Multicharged
Close: Neutralized
q = 11, ηD+ ηIM
q = 9, ηD+ ηIM
q = 7, ηD+ ηIM
q = 5, ηD+ ηIM
q = 3, ηD+ ηIM
q = 1, ηD+ ηIM
q = 0, ηD

348

349 **Fig. 7.**

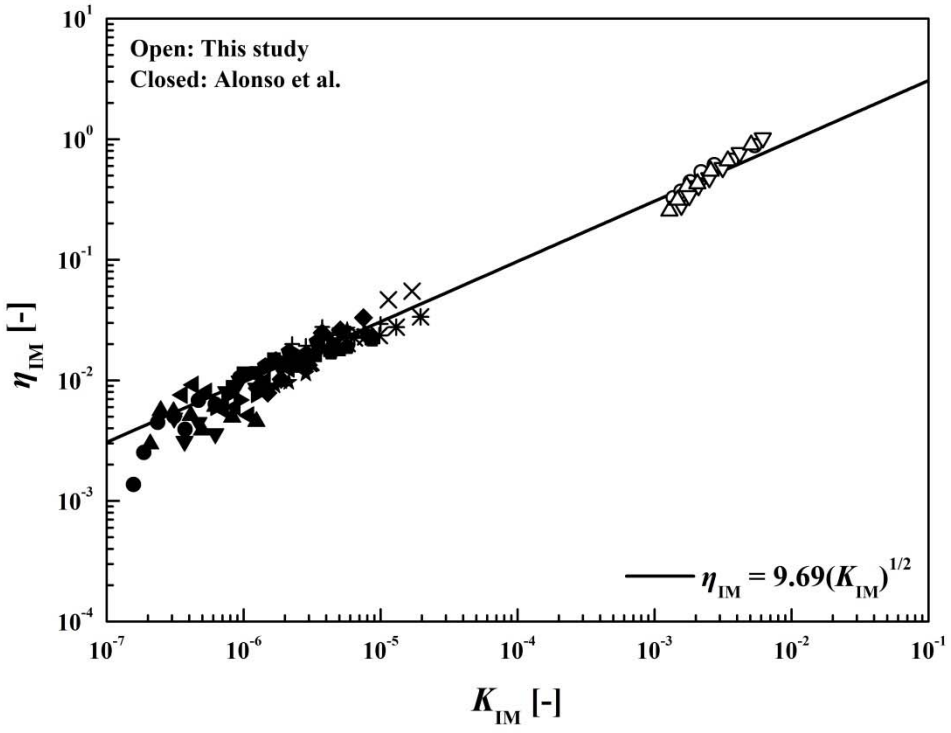
Open: This study
Closed: Alonso et al.
$\eta_{IM} = 9.69(K_{IM})^{1/2}$
η_{IM} [-]
K_{IM} [-]
10^{1}
10^{0}
10^{-1}
10^{-2}
10^{-3}
10^{-4}
10^{-7}
10^{-6}
10^{-5}
10^{-4}
10^{-3}
10^{-2}
10^{-1}

350

351 **Fig. 8.**